






RESEARCH ARTICLE | AUGUST 22 2023

## Chiral-induced spin selectivity in photo-induced electron transfer: Investigating charge and spin dynamics in a master equation framework

Special Collection: [Chiral Induced Spin Selectivity](#)

Emilio Macaluso ; Alessandro Chiesa ; Paolo Santini; Robert Bittl ; Stefano Carretta  



*J. Chem. Phys.* 159, 084301 (2023)

<https://doi.org/10.1063/5.0160149>



View  
Online



Export  
Citation

CrossMark

### Articles You May Be Interested In

Toward quantum sensing of chiral induced spin selectivity: Probing donor–bridge–acceptor molecules with NV centers in diamond

*J. Chem. Phys.* (April 2023)

Development of boron liquid metal ion source for focused ion beam system

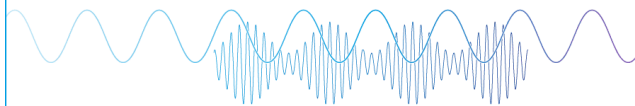
*Journal of Vacuum Science & Technology B: Microelectronics Processing and Phenomena* (January 1987)

Effective spin Hamiltonian for magnetic clusters in presence of S mixing

*Journal of Applied Physics* (May 2003)

Webinar

Boost Your Signal-to-Noise  
Ratio with Lock-in Detection



Sep. 7th – Register now



Zurich  
Instruments

# Chiral-induced spin selectivity in photo-induced electron transfer: Investigating charge and spin dynamics in a master equation framework

Cite as: J. Chem. Phys. 159, 084301 (2023); doi: 10.1063/5.0160149

Submitted: 30 May 2023 • Accepted: 31 July 2023 •

Published Online: 22 August 2023








View Online



Export Citation



CrossMark

Emilio Macaluso,<sup>1</sup>  Alessandro Chiesa,<sup>1,2,3</sup>  Paolo Santini,<sup>1,2,3,a)</sup>  Robert Bittl,<sup>4,b)</sup>   
and Stefano Carretta<sup>1,2,3,c)</sup> 

## AFFILIATIONS

<sup>1</sup>Università di Parma, Dipartimento di Scienze Matematiche, Fisiche e Informatiche, I-43124 Parma, Italy

<sup>2</sup>UdR Parma, INSTM, I-43124 Parma, Italy

<sup>3</sup>INFN-Sezione di Milano-Bicocca, Gruppo Collegato di Parma, Parma 43124, Italy

<sup>4</sup>Fachbereich Physik, Berlin Joint EPR Lab, Freie Universität Berlin, D-14195 Berlin, Germany

**Note:** This paper is part of the JCP Special Topic on Chiral Induced Spin Selectivity.

<sup>a)</sup>Electronic mail: [paolo.santini@unipr.it](mailto:paolo.santini@unipr.it)

<sup>b)</sup>Electronic mail: [robert.bittl@fu-berlin.de](mailto:robert.bittl@fu-berlin.de)

<sup>c)</sup>Author to whom correspondence should be addressed: [stefano.carretta@unipr.it](mailto:stefano.carretta@unipr.it)

## ABSTRACT

Investigating the role of chiral-induced spin selectivity in the generation of spin correlated radical pairs in a photoexcited donor–chiral bridge–acceptor system is fundamental to exploit it in quantum technologies. This requires a minimal master equation description of both charge separation and recombination through a chiral bridge. To achieve this without adding complexity and entering in the microscopic origin of the phenomenon, we investigate the implications of spin-polarizing reaction operators to the master equation. The explicit inclusion of coherent evolution yields non-trivial behaviors in the charge and spin dynamics of the system. Finally, we apply this master equation to a setup comprising a molecular qubit attached to the donor–bridge–acceptor molecule, enabling qubit initialization, control, and read-out. Promising results are found by simulating this sequence of operations assuming realistic parameters and achievable experimental conditions.

Published under an exclusive license by AIP Publishing. <https://doi.org/10.1063/5.0160149>

## I. INTRODUCTION

The study of photo-induced electron transfer (PET) through a chiral bridge is recently receiving a growing amount of attention<sup>1–8</sup> as an ideal, simple test-bed for understanding Chirality-Induced Spin Selectivity (CISS). For instance, it has been shown that magnetic resonance techniques can be exploited to assess the spin wave function after PET of a radical pair generated in donor–chiral bridge–acceptor (D- $\chi$ -A) systems.<sup>9,10</sup> The simplicity of this kind of setup is due to the absence of metallic leads or substrates with large spin–orbit coupling, which otherwise could play an important role in spin selectivity detected via electron transport experiments.<sup>11–13</sup> This simplification will allow us to focus only on the role of the chiral bridge in the CISS effect both in the interpretation of experimental data and as a guide for a microscopic theoretical modeling of the phenomenon.

Moreover, a great interest toward spin-correlated radical pairs, potentially linked by a chiral bridge, is coming from the field of quantum technologies.<sup>8,14–22</sup> In particular, a setup consisting of a D- $\chi$ -A molecule linked to a spin qubit (D- $\chi$ -A-Q hereafter) has been recently proposed as a promising architecture for quantum computing, enabling high-temperature initialization and read-out of a single spin by exploiting spin-selective electron transfer.<sup>8</sup> The high-temperature efficiency of the phenomenon is one of the important advantages it offers for quantum computing applications. For instance, the polarization of the transferred spin can be exploited for initialization of Q even at high temperature, where the qubit spin is completely unpolarized.

Another relevant issue that deserves investigation is the effect of CISS in charge recombination<sup>6,7</sup> through D- $\chi$ -A systems. Spin selectivity is expected to work in both directions, facilitating back-

ward transfer for the opposite spin orientation than forward transfer. By linking spin to charge degrees of freedom, this property can be exploited to activate a spin-to-charge conversion mechanism that unfolds an even more promising quantum computing application, i.e., the readout of single spin.<sup>8</sup>

To gain a deeper understanding of these processes and implement realistic simulations, here, we consider a master equation describing spin-selective electron transfer reactions through suitable “Haberkorn” operators.<sup>23</sup> These reaction operators are defined as projectors on spin states with local spin polarization, expanding on what proposed in Ref. 7. This phenomenological model does not enter into the microscopic origin of the CISS effect and can, therefore, accommodate different forms of the reaction operators, according to developments in the fundamental understanding of CISS that are currently being carried out.<sup>4,5,24</sup>

We simulate both forward and backward charge transfer processes in the presence of spin-selectivity. Remarkably, we find important effects arising from the interplay of the coherent spin dynamics and incoherent charge dynamics involved in the reaction. This allows us to highlight important consequences of introducing spin-polarizing reaction operators in Haberkorn equations and to identify limiting factors and a proper hierarchy of interactions to make these kinds of systems suitable for quantum computing applications.

Finally, we use the spin-selective master equation to simulate an entire quantum computing workflow, from initialization to gates and readout, following the proposal in Ref. 8. We show that the high-temperature initialization of a molecular spin qubit, such as a  $\text{Cu}^{2+}$  complex,<sup>25</sup> coupled to the acceptor spin is possible via a simple sequence of resonant microwave pulses, overcoming an important drawback of molecular qubits.<sup>26</sup> We also implemented one-qubit gates with high fidelity in times much shorter than decoherence times typical of molecular systems.<sup>27–31</sup> Finally, by inducing backward transfer via an external tool such as an electric field, we reproduce the steps needed to convert the spin information of the qubit to charge information on the donor, effectively enabling high-temperature readout of the quantum state of a single spin, a major technological challenge.

## II. MODEL SYSTEM AND KINETIC EQUATIONS

First, we need to set up master equations describing forward and backward electron-transfer reactions in the presence of a chiral bridge. For both reactions, we chose to adapt the conventional Haberkorn equation of motion for the spin density matrix<sup>23,32–34</sup> and to include CISS-induced spin selectivity in both electron transfer (ET) and recombination through spin-polarizing reaction operators. This was first done in Ref. 7 to model the dynamics of the radical pair in the context of electron paramagnetic resonance (trEPR) detection. Here, we follow the same approach, but include besides the charge-separated stage (CS)<sup>34,35</sup> the initial photo-excited stage (PE) and the charge-recombined stage (CR) in the kinetic equations, as shown schematically in Fig. 1. This labeling is based on the sequence of the electron transfer events involved in the reactions. PE labels the states in which one electron of the neutral donor is promoted to the LUMO, CS labels the states with the former excited electron transferred to the acceptor, and CR labels the neutral states (of donor and acceptor) after charge recombination. This implicitly

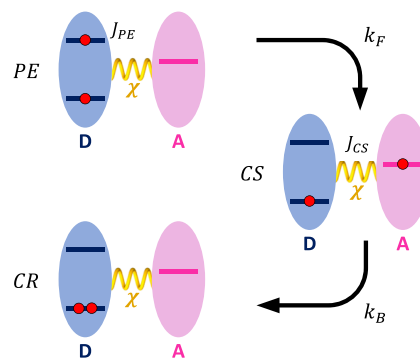


**FIG. 1.** Schematic representation of the three different charge transfer stages we considered in our model. The two ellipsoids represent donor (D, blue shaded) and acceptor (A, pink shaded), while red circles indicate the electrons. Spin–spin interactions  $J_{PE}$  and  $J_{CS}$  are highlighted in the respective charge transfer stages. The CR state is supposed to relax to its ground state, which can be photoexcited again.

assumes that different spin states on the donor are in one-to-one correspondence with different charge distributions. Quantum states at the three charge transfer stages are labeled as  $|\sigma\rangle_\phi$ , where  $\sigma$  describes the two-electron spin state and  $\phi$  denotes the stages PE, CS, and CR in the ET sequence in Fig. 1. We also assume properly orthogonalized spatial functions for the different involved spin states but omit them for simplicity. Each of the three charge transfer stages is described by a different spin density matrix, allowing us to introduce specific coherent spin dynamics on each stage. The following is the general form of the master equations, which describes charge separation from PE to CS and charge recombination from CS to CR by

$$\dot{\rho}_{PE} = -\frac{i}{\hbar}[\hat{H}_{PE}, \rho_{PE}] - \frac{k_F}{2}\{\hat{P}_F, \rho_{PE}\}, \quad (1a)$$

$$\dot{\rho}_{CS} = -\frac{i}{\hbar}[\hat{H}_{CS}, \rho_{CS}] + k_F\hat{P}_F\rho_{PE}\hat{P}_F - \frac{k_R}{2}\{\hat{P}_B, \rho_{CS}\}, \quad (1b)$$

$$\dot{\rho}_{CR} = -\frac{i}{\hbar}[\hat{H}_{CR}, \rho_{CR}] + k_R\hat{P}_B\rho_{CS}\hat{P}_B, \quad (1c)$$

where  $\rho_\phi = |\sigma\rangle_\phi\langle\sigma|_\phi$ .

We stress that, for the proposed quantum computing applications, we are only interested in whether the CS state persists or charge recombination has occurred, independent of the spin state of CR, which acts only as a sink in our simulations. This corresponds to evaluating the charge on the donor, i.e.,  $\text{Tr}\rho_{CS}$ . Hence, Eq. (1c) does not need to be explicitly solved and we omit it hereafter.

Charge separation and recombination are described as fully incoherent processes by the electron transfer rates  $k_F$  and  $k_R$ , respectively.<sup>32–34</sup>  $\hat{P}_F$  and  $\hat{P}_B$  are the reaction operators responsible of spin selective charge transfer, whose specific form is introduced in the next sections. Spin relaxation and dephasing could be incorporated in Eq. (1) by appropriate relaxation and dephasing operators; however, we neglect them for simplicity and comment on this choice below. Coherent spin dynamics are computed through the spin Hamiltonians  $\hat{H}_i$  of the corresponding charge transfer stages. In

particular,  $\hat{H}_i$  includes Zeeman and spin–spin interaction terms, defined as

$$\hat{H}_{PE} = g_D \mu_B \mathbf{B} \cdot (\mathbf{S}_1 + \mathbf{S}_2) + \mathbf{S}_1 \cdot \mathbf{J}_{PE} \cdot \mathbf{S}_2, \quad (2a)$$

$$\hat{H}_{CS} = g_D \mu_B \mathbf{B} \cdot \mathbf{S}_1 + g_A \mu_B \mathbf{B} \cdot \mathbf{S}_2 + \mathbf{S}_1 \cdot \mathbf{J}_{CS} \cdot \mathbf{S}_2, \quad (2b)$$

where  $g_D$  and  $g_A$  are the  $g$ -factors for donor and acceptor, respectively, assumed isotropic and equivalent in different charge transfer stages, for sake of simplicity. The model can be easily generalized to anisotropic and charge-state dependent  $g$  tensors.  $\mathbf{S}_i = (S_{i,x}, S_{i,y}, S_{i,z})$  are the spin operators for the two electrons, labeled as  $i = 1, 2$ . More specifically, in the CS stage,  $i = 1$  represents the electron that does not undergo transfer and  $i = 2$  represents the moving electron. Spin–spin coupling tensors  $\mathbf{J}_i$  include both isotropic exchange as well as dipolar interactions. Magnetic field  $\mathbf{B}$  is always considered parallel to the chiral axis, i.e., the line joining the two sites.

In Secs. III and IV, we separately simulate charge separation and recombination by numerically solving this set of equations. To this aim, we will consider only a subset of Eqs. (1) at a time. This allows us to more clearly address the implications of charge and spin dynamics in the two separate reactions. This choice is made possible by the very different transfer rates usually characterizing charge separation and recombination in this kind of system. In fact, typical charge separation times are in the 100 ps–few ns range, while spontaneous recombination occurs on the  $\mu$ s and even longer time scales, thus being completely ineffective in the forward process.<sup>36</sup>

### III. CHARGE SEPARATION

Let us begin by considering the forward (charge separation) process in the presence of “perfect CISS effect,” leading to 100% polarization of the transferred electron in the radical pair. Hence, we consider Eqs. (1a) and (1b), in which we suppose, without loss of generality, that the CISS reaction operator is  $\hat{P}_F = \hat{P}_\uparrow = |\uparrow\uparrow\rangle\langle\uparrow\uparrow| + |\downarrow\uparrow\rangle\langle\downarrow\uparrow|$ , thus selecting the  $|\uparrow\rangle$  state of the transferred spin. Therefore, Eq. (1) reads

$$\dot{\rho}_{PE} = -\frac{i}{\hbar} [\hat{H}_{PE}, \rho_{PE}] - \frac{k_F}{2} \{\hat{P}_\uparrow, \rho_{PE}\}, \quad (3a)$$

$$\dot{\rho}_{CS} = -\frac{i}{\hbar} [\hat{H}_{CS}, \rho_{CS}] + k_F \hat{P}_\uparrow \rho_{PE} \hat{P}_\uparrow, \quad (3b)$$

where the spin Hamiltonians of the two stages induce a coherent evolution through on-site exchange coupling  $J_{PE}$  and dipolar interaction  $J_{CS}$  between the donor and acceptor.

In the simulations, we include reasonable values for all the parameters in the spin Hamiltonians, namely, a strong on-site isotropic exchange coupling on the donor  $J_{PE} = -1$  eV, slightly different  $g$ -factors  $g_D = 2 - \varepsilon$  and  $g_A = 2 + \varepsilon$  ( $\varepsilon = 0.001$ ) and the dipolar coupling  $J_{CS}$  computed for a donor–acceptor distance  $d = 20$  Å within the point-dipole approximation. We assume fast photo-excited electron transfer  $k_F = 5$  ns<sup>-1</sup>, as occurs in spin-correlated radical pairs.<sup>36</sup> The magnetic field (parallel to the chiral bridge) is  $B = 1.05$  T, large enough to ensure good spin state factorization in the CS stage, an important requirement for quantum computing applications

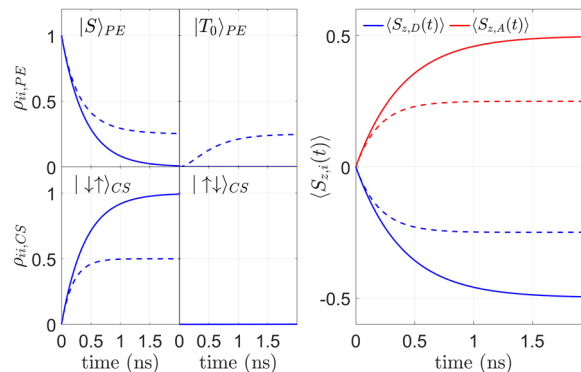


**FIG. 2.** Left: populations of the  $\langle S_{z,\text{tot}} \rangle = 0$  spin states in the PE charge transfer stage (top row) and in the CS charge transfer stage (bottom row) as function of time. Here,  $|S\rangle = (|\uparrow\downarrow\rangle - |\downarrow\uparrow\rangle)/\sqrt{2}$  and  $|T_0\rangle = (|\uparrow\downarrow\rangle + |\downarrow\uparrow\rangle)/\sqrt{2}$ . Right: spin polarization  $\langle S_{z,i} \rangle$  computed on both sites ( $i = D, A$ ) as a function of time. Solid lines are computed with the realistic  $J_{PE} = -1$  eV, ultimately leading to complete transfer of population from  $\rho_{PE}$  to  $\rho_{CS}$ . We also report results for the unrealistic case of  $J_{PE} = 0$  (dashed lines) to exclude the coherent dynamics in PE states from the simulations, thus highlighting its effect on the charge transfer process in the presence of a spin-selective reaction operator.

(see Sec. V). The results of our simulations are shown in Fig. 2, where populations of  $\langle S_z \rangle = \langle S_{z,1} + S_{z,2} \rangle = 0$  spin states and local spin polarization  $\langle S_{z,i} \rangle$  on both sites are reported as a function of time, up to 2 ns. The system was initialized in a photo-excited singlet spin state  $|S\rangle = (|\uparrow\downarrow\rangle - |\downarrow\uparrow\rangle)/\sqrt{2}$ , i.e.,  $\rho_{PE}(0) = |S\rangle_{PE}\langle S|_{PE}$ .

The most relevant result is that the final state is characterized by  $\langle S_{z,A} \rangle = -\langle S_{z,D} \rangle = 0.5$ , i.e., maximum local spin polarization on both D and A, leading in turn to maximum overall spin polarization  $p = \langle S_{A,z} \rangle - \langle S_{D,z} \rangle = 1$ . Moreover, the charge is completely transferred from D to A. This could appear surprising since the evolution induced only by the Haberkorn reaction operators would lead to only a 50% charge transfer from D to A, as only half of the initial singlet population is transferred by the  $\hat{P}_\uparrow$  reaction operator. This complete charge transfer and maximum polarization are due to the fast coherent dynamics ruled by  $J_{PE}$ , which mixes  $|\downarrow\uparrow\rangle_{PE}$  and  $|\uparrow\downarrow\rangle_{PE}$ , thus ensuring that there is always sufficient population in the  $|\downarrow\uparrow\rangle_{PE}$  state that eventually undergoes charge transfer. In order to highlight that this effect originates exactly from  $J_{PE}$ , we compare in Fig. 2 realistic simulations of Eq. (3) with  $J_{PE} = -1$  eV with the hypothetical case of  $J_{PE} = 0$ . In the latter case the evolution is dominated by the reaction operator, which results, as anticipated, in incomplete charge transfer and polarization (dashed lines). Conversely, the coherent evolution in the CS stage (included in our simulations) is much slower and hence it does not affect the charge separation reaction. As discussed below, it plays a much more central role in recombination, given the longer time scale of this process.

Note that our choice for the reaction operator  $\hat{P}_F = \hat{P}_\uparrow = |\uparrow\uparrow\rangle\langle\uparrow\uparrow| + |\downarrow\uparrow\rangle\langle\downarrow\uparrow|$  is only an assumption due to the so far incomplete understanding of the microscopic origin of CISS in PET. Other choices are possible and can be included in Eq. (1). A reasonable alternative would be  $\hat{P}_F = |\downarrow\uparrow\rangle\langle\downarrow\uparrow|$ , as proposed in Ref. 7. The main difference introduced by this choice compared to the former would be excluding charge separation or recombination through  $\langle S_z \rangle \neq 0$

spin states. Hence, no qualitative difference is expected for the simulations of Fig. 2, but a different dynamics could arise for initial spin states different from the singlet.

#### IV. CHARGE RECOMBINATION

We now consider the backward (charge recombination) process, described by a simplified version of Eq. 1(b),

$$\dot{\rho}_{CS} = -\frac{i}{\hbar}[\hat{H}_{CS}, \rho_{CS}] - \frac{k_R}{2}\{\hat{P}_\downarrow, \rho_{CS}\}, \quad (4)$$

under the assumption the CISS effect selects the opposite spin orientation for the backward compared to the forward reaction through the reaction operator  $\hat{P}_\downarrow = |\uparrow\downarrow\rangle\langle\uparrow\downarrow| + |\downarrow\downarrow\rangle\langle\downarrow\downarrow|$ . As noted above, the population of CR is simply given by the trace conservation of the overall density matrix, while its spin state is irrelevant.

Figure 3 shows the results of numerical integration of Eq. (4), performed with the same  $J_{CS}$  as before, a recombination rate of  $k_R = 1 \mu\text{s}^{-1}$  and starting from the fully charge-separated initial state  $\rho_{CS}(0) = |\sigma_0\rangle_{CS}\langle\sigma_0|_{CS}$ , in which  $|\sigma_0\rangle_{CS} = (|\uparrow\uparrow\rangle_{CS} + |\downarrow\downarrow\rangle_{CS})/\sqrt{2}$ . This choice for the initial state allows us to investigate the effect of spin selectivity in charge recombination. To highlight spin selectivity effects, we omit spin relaxation and dephasing, which, in general, might be relevant on the studied time scale.

The most striking difference between Figs. 2 and 3 is the loss of population from the  $|\downarrow\downarrow\rangle_{CS}$  state [Fig. 3(a)], which should be prevented by the specific form of  $\hat{P}_\downarrow$ . However, the spin–spin interaction in  $\hat{H}_{CS}$  couples and mixes  $|\uparrow\downarrow\rangle_{CS}$  and  $|\downarrow\uparrow\rangle_{CS}$ , similarly to  $J_{PE}$  in the charge separation reaction. Since one of the two coupled states is affected by the reaction operator  $\hat{P}_\downarrow$ , this continuous mixing effectively leads to a loss of population from  $|\uparrow\downarrow\rangle_{CS}$  and, therefore, to  $\text{Tr} \rho_{CR} > 1/2$  [Fig. 3(b)] and a corresponding loss of spin polarization [Fig. 3(c)]. This effect disappears if we remove  $J_{CS}$  from the simulations (dashed lines in Fig. 3).

We note that with the set of parameters above, this harmful non-spin-selective recombination is significantly slower than  $k_R$ ,

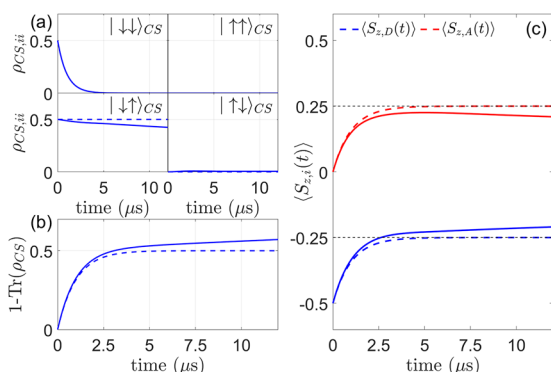


**FIG. 3.** (a) Populations of the spin states in the CS charge transfer stage and (b) population of recombined states as a function of time. Solid and dashed lines are computed with  $J_{CS} = 0$  and  $J_{CS} \neq 0$ , respectively. (c) Spin polarization  $\langle S_{z,i} \rangle$  computed on both sites ( $i = D, A$ ) as a function of time. Solid and dashed lines are computed with  $J_{CS} = 0$  and  $J_{CS} \neq 0$ , respectively.

and hence, it only yields a limited loss of spin polarization. Nevertheless, several parameters can improve or hinder the effectiveness of this channel. In the specific case of Fig. 3, the small  $\Delta g = g_A - g_D$  and slow  $k_R$  are both favorable conditions for the onset of a non-spin polarizing recombination. In order to preserve spin polarization in charge recombination, we can adopt one of the following approaches:

- (1) Reducing the intensity of the spin–spin interaction  $J_{CS}$  by increasing the distance  $d$  between the donor and acceptor. This directly limits the coherent spin dynamics of the CS state but also suppresses  $k_F$  and  $k_R$  rates.<sup>37</sup>
- (2) Increasing the energy gap between the spin states  $|\uparrow\downarrow\rangle_{CS}$  and  $|\downarrow\uparrow\rangle_{CS}$  coupled by  $J_{CS}$ , thus effectively suppressing their evolution. This can be achieved by increasing the difference between the two  $g$ -factors, as well as by introducing additional interactions in the spin Hamiltonian (see below).
- (3) Accelerating the recombination process. Indeed, unwanted spin recombination will be less effective if charge recombination takes place in a shorter time scale than coherent spin dynamics. Moreover, for  $k_R \gg J_{CS}/\hbar$ , spin selective recombination would be restored by the quantum Zeno effect, which results in a significant slow-down of coherent evolution of a quantum state in the presence of much faster incoherent processes (see below).

Although the loss of spin polarization may appear as a severely limiting factor for potential applications in quantum technologies (e.g., reducing spin selectivity for state readout), in Sec. V, we show that including a molecular spin qubit coupled to the acceptor spin, can entirely suppress the detrimental effect of  $J_{CS}$ .

Before moving to quantum computing applications, we examine an interesting aspect of these simulations, namely, the possibility of exploring the onset of the quantum Zeno effect (QZE) by varying the recombination rate  $k_R$ . Due to QZE, continuous measurement of a quantum system halts its coherent evolution. Analogously, QZE appears also in the case of continuous strong coupling to a noisy environment or in electron transfer described through Haberkorn reaction operators, as already predicted in Ref. 33.

This mechanism was not relevant in the charge separation step described in Sec. III, since the large  $J_{PE}/\hbar \gg k_F$  led to extremely fast coherent spin dynamics. Conversely, the typically slow coherent evolution induced by  $J_{CS}$  in the CS stage opens up the possibility of observing QZE. The impact of QZE on charge recombination is explored in Fig. 4, where we present spin state populations and spin polarizations on D and A as a function of  $k_R t$  for both  $k_R = 1 \mu\text{s}^{-1}$  and the much faster rate  $k_R = 1 \text{ns}^{-1}$ . The other parameters and the initial state are the same as in Fig. 3. We note the onset of QZE for large values of  $k_R$ , combined with the slower coherent dynamics typical of the CS stage. Indeed, the coherent evolution induced by  $J_{CS}$  is practically suppressed when  $k_R \gg J_{CS}/\hbar$ , thus avoiding the population of the  $|\uparrow\downarrow\rangle_{CS}$  state and, hence, preserving spin polarization during charge recombination. This is clearly shown in Fig. 4 (right). Besides their fundamental interest to explore the QZE, these considerations are also important for applications in quantum technologies, where spin-selective charge transfer is important.

However, fast recombination rates are not typical for this kind of system, in which recombination usually takes place over the



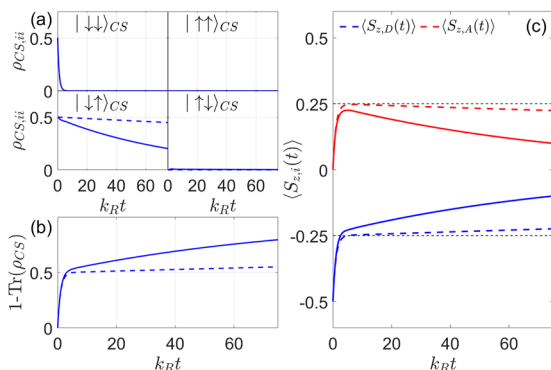


**FIG. 4.** (a) Populations of the spin states in the CS charge transfer stage and (b) population of recombined states as a function of time. Solid and dashed lines are computed with  $k_R = 1 \mu\text{s}^{-1}$  and  $k_R = 1 \text{ns}^{-1}$ , respectively. (c) Spin polarization  $\langle S_{z,i} \rangle$  computed on both sites ( $i = D, A$ ) as a function of time. Solid and dashed lines are computed with  $k_R = 1 \mu\text{s}^{-1}$  and  $k_R = 1 \text{ns}^{-1}$ , respectively. In all plots, time has been multiplied by  $k_R$  in the  $x$  axes, in order to keep the time window comparable to each corresponding recombination rate.

1–10  $\mu\text{s}$  time scale.<sup>20,38</sup> Nevertheless, since charge transfer rates are determined by the energy level structure of the system, they can be modulated by external stimuli, such as laser pulses<sup>39</sup> or electric fields. The dependence of charge transfer rates on an applied electric field has been theoretically estimated in Ref. 40 through Marcus' theory for adiabatic electron transfer, obtaining an exponential growth of charge transfer rates with an increasing electric field. Hence, it is reasonable to assume a swift growth of charge transfer rates over multiple orders of magnitude, leading to effects comparable to those simulated in Fig. 4. The capability of controlling recombination rates is also crucial for applications in the field of quantum computing, as expanded upon in Sec. V.

## V. APPLICATIONS IN QUANTUM COMPUTING

The applications of CISS-mediated electron transfer in quantum technologies proposed in Ref. 8 involve the addition of a

molecular spin qubit  $Q$  ( $S_Q = 1/2$ ) to the D- $\chi$ -A system. While individual molecular spins usually need extremely low temperatures ( $\sim 10$  mK) for initialization and are extremely difficult to read, this D- $\chi$ -A-Q hardware exploits CISS and its effectiveness at high temperatures to circumvent these problems. In fact, by using resonant microwave pulses, it is possible to transfer spin polarization from the acceptor to the qubit, exploiting spin transitions of the system in the CS stage. In addition, qubit state readout can be implemented by first transferring spin polarization back from qubit to the acceptor and then exploiting the spin-selective charge recombination through a chiral bridge to transform the spin information initially stored in the qubit to charge information on the donor site, much easier to assess.

In this section, we simulate initialization, quantum gates, and readout of a molecular qubit as proposed in Ref. 8 by numerically solving a generalization of Eq. (1). Adapting Eq. (1) to this kind of system only requires the inclusion of an additional spin  $S_Q$  coupled to the acceptor spin  $S_A$  through exchange coupling  $J_{AQ}$ . We report in Fig. 5 the simulation of various quantum computing steps on the qubit, which also involve the (controlled) charge dynamics discussed in Secs. III and IV. The employed parameters are those used before for the D- $\chi$ -A system; whereas for the qubit, we assume a diagonal  $g$  tensor  $g_Q = (2.1, 2.1, 2.3)$  (as typical for  $\text{Cu}^{2+}$  complexes, see e.g., Ref. 25), which resonates in the Q band at the used field  $B = 1.05$  T, and an isotropic exchange  $J_{AQ} = -0.02 \text{cm}^{-1}$ . The assumed charge separation and recombination rates are:  $k_F = 5 \text{ns}^{-1}$  and  $k_R = 1 \mu\text{s}^{-1}$ , except for the last step in which  $k_R$  exponentially grows up to  $k_R = 1 \text{ns}^{-1}$ . Gaussian-shaped resonant pulses are used for qubit manipulations, with peak amplitude  $B_1 = 50$  G. These parameters were chosen keeping in mind important aspects for the performance of the whole system. The condition  $(g_Q - g_A)\mu_B B \gg J_{AQ}$  provides good factorization of the spin states, which is important for the definition of sound qubit states. Moreover, the additional energy splitting induced by  $J_{AQ}$  on the acceptor makes coherent evolution due to the transversal component of  $J_{CS}$  practically ineffective. Hence, this D- $\chi$ -A-Q system is naturally protected from unwanted charge recombination. For the following simulations, we consider an initial singlet state on the photo-excited D-A system and  $\langle S_{z,Q}(0) \rangle = 0$ , i.e., negligible polarization of the qubit, as would

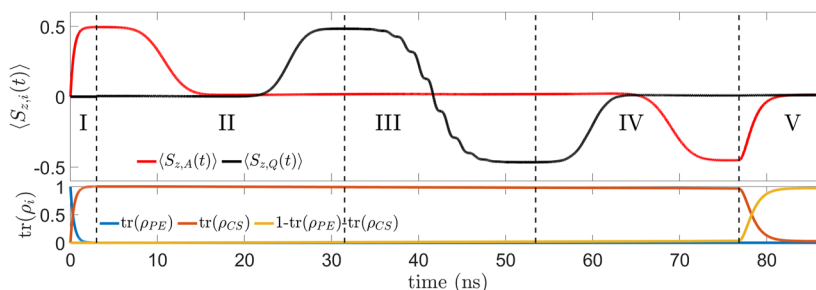


**FIG. 5.** Top: spin polarization  $\langle S_{z,i} \rangle$  computed on acceptor and qubit sites ( $i = A, Q$ ) as a function of time. Bottom: populations of charge transfer stages as a function of time. The five time sections in which both plots are divided are: charge separation (I), qubit initialization (II),  $R_y(\pi)$  gate on the qubit (III), reverse initialization (IV), and stimulated charge recombination (V). At the end of step V the qubit state is found in an equivalent mixture of  $|\downarrow\rangle_Q$  and  $|\uparrow\rangle_Q$  after complete charge recombination. The fidelity of the whole procedure (i.e., the overlap between the target state and the actual state after simulating the time evolution) is 0.99.

occur at room temperature. The corresponding initial state is given by

$$\rho_{PE}(0) = |S\rangle_{PE}\langle S|_{PE} \otimes \frac{|\downarrow\rangle_Q\langle\downarrow|_Q + |\uparrow\rangle_Q\langle\uparrow|_Q}{2}, \quad (5)$$

where the last spin represents the qubit. Note that the entire simulation works also for a mixture with thermal populations ( $\langle S_{z,Q}(0) \rangle \neq 0$ ) or a coherent superposition of qubit spin states.

Results of the full simulation are reported in Fig. 5, where  $\langle S_{z,A}(t) \rangle$  and  $\langle S_{z,Q}(t) \rangle$  are shown in the top panel and occupancy of the three charge transfer stages is plotted in the bottom panel as a function of time. We now describe in more detail the five steps of the simulation in Fig. 5, emphasizing the strengths and weaknesses of the proposed model and architecture:

- (I) **Charge separation** is simulated exactly as shown in Fig. 2, leading to CISS-induced full polarization of the acceptor within 3 ns.
- (II) **Qubit initialization** is accomplished with two consecutive resonant pulses addressing the spin transitions  $|\downarrow\rangle_{CS} \otimes |\uparrow\rangle_Q \leftrightarrow |\downarrow\rangle_{CS} \otimes |\downarrow\rangle_Q$  and  $|\downarrow\rangle_{CS} \otimes |\downarrow\rangle_Q \leftrightarrow |\downarrow\rangle_{CS} \otimes |\uparrow\rangle_Q$ , effectively transferring spin polarization from the acceptor to the qubit as explained in Refs. 8 and 9. Note that during this step, the  $|\downarrow\rangle_A$  spin state of the acceptor starts being populated, thus activating slow spin selective charge recombination, as can be seen from the slight population variation in Fig. 5 (bottom) in steps II–IV. However, this charge recombination is very slow compared to coherent spin manipulation and does not lead to a significant error at the end of the simulation.
- (III) **One qubit gate** can now be implemented on the initialized qubit via resonant pulses. In Fig. 5, we show a  $R_y(\pi)$  gate inverting the polarization of the qubit, obtained with two resonant pulses between the spin states  $|\downarrow\rangle_{CS} \otimes |\downarrow\rangle_Q \leftrightarrow |\downarrow\rangle_{CS} \otimes |\uparrow\rangle_Q$  and  $|\downarrow\rangle_{CS} \otimes |\downarrow\rangle_Q \leftrightarrow |\downarrow\rangle_{CS} \otimes |\uparrow\rangle_Q$ , implemented in parallel for optimal performance.
- (IV) **Reverse initialization.** After qubit manipulations, we swap the qubit state with the acceptor. This can be achieved by performing the two pulses of step II in reverse order. Since in step (III) we performed a  $\pi$  gate on the qubit, here we obtain inverse polarization of the acceptor spin with respect to the initial CISS polarization.
- (V) **Charge recombination.** Once the state of the qubit has been swapped to the acceptor, we induce spin-selective charge recombination to convert spin into charge and, hence, access the former state of the qubit by measuring the final charge on the donor. In particular, the ideal CISS effect will only allow the  $|\downarrow\rangle$  component of the wave-function to recombine (through the reaction operator  $\hat{P}_\downarrow$ ). As a consequence, the two states of the qubit we want to readout ( $|\uparrow\rangle_Q$  or  $|\downarrow\rangle_Q$  at the end of point III) will result in different charge states of D and A—either neutral if recombination had occurred or both still charged if recombination is blocked by CISS. Hence, a measurement of the donor's charge state (with a charge detector close to D) allows us to access the former spin state of the qubit.

Note that spontaneous recombination would require multiple  $\mu$ s. Hence, in this step, we consider a fast-changing  $k_R$  that exponentially varies over  $\approx 1$  ns from  $k_R = 1 \mu\text{s}^{-1}$  to  $k_R = 1 \text{ns}^{-1}$ , compatible with a quick variation of an applied electric field.<sup>40</sup> This allows us to significantly speed-up charge recombination, thus completing it in times much shorter than the acceptor spin relaxation and of non-spin-selective recombination (also thanks to the quantum Zeno effect). This is needed for the readout scheme to work properly. Below, we discuss the implications of longer or non-spin-selective recombination times on the effectiveness of the scheme. Final readout of the charge state of the donor can then be realized by a sensitive electrometer,<sup>41</sup> whose specific realization is beyond the scope of these simulations.

In summary, the calculation based on realistic parameters documents an efficient readout with complete recombination and an error less than 1%. The inclusion of dephasing effects with reasonable  $T_2$  (a few hundred of ns on D and A, a few  $\mu$ s on Q) only marginally increases this error. This approach to qubit readout can be extended to a full tomography of the quantum state by adding rotations on the qubit before steps IV and V. Indeed, the high fidelity of coherent manipulation with microwave pulses ensures a full control of the qubit in step III.

The most relevant sources of readout error can be associated with hardware limitations in experimental charge measurement or, more importantly, to imperfect spin selectivity in the charge transfer processes, leading to  $<100\%$  spin polarization. We stress that CISS has been experimentally detected in electron transfer, producing spin polarization as large as 80%,<sup>1</sup> and very high values have been demonstrated in transport setups.<sup>42–45</sup> However, values of spin polarization way below 100% are predicted by the theoretical mechanism proposed in Ref. 5. Hence, the possibility of having reaction operators that do not project on perfectly spin-polarized spin states has to be considered. To this end, it is possible to include “imperfect CISS effect” using the following reaction operator, defined for both charge separation ( $F$ ) and recombination ( $R$ ):

$$\hat{P}_{F,R} = p_{\text{CISS}}\hat{P}_{\uparrow,\downarrow} + (1 - p_{\text{CISS}})\hat{P}_S, \quad p_{\text{CISS}} \in [0, 1], \quad (6)$$

where  $\hat{P}_S$  is the reaction operator projecting on the singlet spin state, acting as a non-spin-selective channel for charge transfer. The spin polarization efficiency of CISS is represented by  $p_{\text{CISS}}$ , which is the fraction of charge transfer that takes place through the spin-polarizing channel described by the reaction operator  $\hat{P}_{\uparrow,\downarrow}$ . Its limiting cases are “perfect CISS effect” for  $p_{\text{CISS}} = 1$  and non-spin polarizing charge transfer for  $p_{\text{CISS}} = 0$ .

By simulating charge separation as in Sec. III and implementing the reaction operator defined in Eq. (6) with  $p_{\text{CISS}} = 0.9$ , we obtain a maximum polarization on the acceptor  $\langle S_{z,A} \rangle = 0.4$ . Hence, the value of  $p_{\text{CISS}}$  has a dominant impact on qubit initialization and, consequently, on qubit manipulation and readout. Nonetheless, experimental evidences of CISS are very promising, and even better performances for these systems can be predicted when taking into account further developments in determining the most suitable molecules. In addition, the proposed scheme theoretically compares well to molecular qubit readout alternatives, for which efficient readout is still a major challenge to overcome.<sup>46–48</sup>

An “imperfect CISS effect” can alternatively be modeled using the reaction operators defined in Ref. 7 as  $\hat{P}_R(\chi) = |\psi(\chi)\rangle\langle\psi(\chi)|$ , where

$$|\psi(\chi)\rangle = \cos(\chi/2)|S\rangle + \sin(\chi/2)|T_0\rangle, \quad (7)$$

with limiting cases  $\chi = \pm\pi/2$ , leading to 100% CISS, and  $\chi = 0$ , leading to no spin polarization. This alternative formulation yields qualitatively analogous results for our protocol, limiting, however, spin-selective recombination to the subspace  $\langle S_{z,DA} \rangle = 0$ . Hence, in that case, microwave pulses should be used to rotate spins of the DA pair before inducing spin-selective recombination.

## VI. CONCLUSIONS

By performing numerical simulations of both charge and spin dynamics of D- $\chi$ -A and D- $\chi$ -A-Q systems, we show CISS to be promising as an enabling technology for quantum applications. We find a good performance of the simulated system for both qubit state initialization and readout when using realistic parameters.

To achieve this, we have used a simple extension of Haberkorn equations to treat forward and backward charge transfer in the presence of spin selectivity. Exploiting a large external magnetic field parallel to the chiral axis we obtain the spin state factorization needed to preserve spin polarization over time in the charge separated state, which would otherwise quickly oscillate under the influence of the transverse component of spin-spin coupling in presence of a smaller field. Moreover, the coupling of the donor-acceptor spin system to a molecular qubit induces a further quenching of the coherent evolution responsible for non-spin-selective charge recombination. In addition, the theoretical framework of Haberkorn's equations, given its phenomenological nature, is very flexible in accommodating alternative forms of spin-selective reaction operators. This will allow to adapt their form once microscopic models of CISS in electron transfer will be developed.<sup>5</sup>

Our findings on the interplay of incoherent and coherent dynamics and the subsequent emergence of the quantum Zeno effect are useful in quantum computing applications. In addition, they could be relevant to rationalize experiments for the detection of CISS in electron transfer.<sup>2</sup> As an example, time-resolved EPR has already been proposed<sup>4,7,9</sup> as a key experimental tool in this field, with some experiments already being performed on D- $\chi$ -A systems.<sup>10</sup> Given the technique sensitivity only to the charge-separated state and its capability to probe the spin wave function of the system as a function of time, trEPR spectra are influenced by both charge and spin dynamics, making our considerations in Sec. IV useful in data interpretation.

## ACKNOWLEDGMENTS

This work has received funding from the Horizon Europe Program through the ERC-Synergy project CASTLE (Project No. 101071533), from the European Union-NextGenerationEU, PNRR MUR Project No. PE0000023-NQSTI, from the Italian Ministry of Education and Research (MUR) through PRIN Project 2017 Grant No. CR5WCH Q-chiSS “Quantum detection of chiral-induced spin selectivity at the molecular level,” from the European

Union's Horizon 2020 research and innovation program (FET-OPEN project FATMOLS) under Grant Agreement No. 862893 and from Fondazione Cariparma.

## AUTHOR DECLARATIONS

### Conflict of Interest

The authors have no conflicts to disclose.

### Author Contributions

**E. Macaluso:** Formal analysis (equal); Investigation (equal); Methodology (equal); Writing – original draft (equal). **A. Chiesa:** Conceptualization (equal); Formal analysis (equal); Investigation (equal); Methodology (equal); Writing – review & editing (equal). **P. Santini:** Methodology (equal); Supervision (equal); Writing – review & editing (equal). **R. Bittl:** Funding acquisition (equal); Methodology (equal); Supervision (equal); Writing – review & editing (equal). **S. Carretta:** Conceptualization (equal); Funding acquisition (equal); Methodology (equal); Supervision (equal); Writing – review & editing (equal).

### DATA AVAILABILITY

The data that support the findings of this study are available from the corresponding author upon reasonable request.

## REFERENCES

- I. Carmeli, K. S. Kumar, O. Heifler, C. Carmeli, and R. Naaman, “Spin selectivity in electron transfer in photosystem I,” *Angew. Chem., Int. Ed.* **53**, 8953–8958 (2014).
- L. A. Völker, K. Herb, E. Janitz, C. L. Degen, and J. M. Abendroth, “Toward quantum sensing of chiral induced spin selectivity: Probing donor–bridge–acceptor molecules with NV centers in diamond,” *J. Chem. Phys.* **158**, 161103 (2023).
- J. M. Abendroth, D. M. Stemer, B. P. Bloom, P. Roy, R. Naaman, D. H. Waldeck, P. S. Weiss, and P. C. Mondal, “Spin selectivity in photoinduced charge-transfer mediated by chiral molecules,” *ACS Nano* **13**, 4928–4946 (2019).
- T. P. Fay, “Chirality-induced spin coherence in electron transfer reactions,” *J. Phys. Chem. Lett.* **12**, 1407–1412 (2021).
- T. P. Fay and D. T. Limmer, “Origin of chirality induced spin selectivity in photoinduced electron transfer,” *Nano Lett.* **21**, 6696–6702 (2021).
- T. P. Fay and D. T. Limmer, “Spin selective charge recombination in chiral donor–bridge–acceptor triads,” *J. Chem. Phys.* **158**, 194101 (2023).
- J. Luo and P. J. Hore, “Chiral-induced spin selectivity in the formation and recombination of radical pairs: Cryptochrome magnetoreception and EPR detection,” *New J. Phys.* **23**, 043032 (2021).
- A. Chiesa, A. Privitera, E. Macaluso, M. Mannini, R. Bittl, R. Naaman, M. R. Wasielewski, R. Sessoli, and S. Carretta, “Chirality-induced spin selectivity: An enabling technology for quantum applications,” *Adv. Mater.* **35**, 2300472 (2023).
- A. Chiesa, M. Chizzini, E. Garlatti, E. Salvadori, F. Tacchino, P. Santini, I. Tavernelli, R. Bittl, M. Chiesa, R. Sessoli, and S. Carretta, “Assessing the nature of chiral-induced spin selectivity by magnetic resonance,” *J. Phys. Chem. Lett.* **12**, 6341–6347 (2021).
- A. Privitera, E. Macaluso, A. Chiesa, A. Gabbani, D. Faccio, D. Giuri, M. Briganti, N. Giaconi, F. Santanni, N. Jarmouni, L. Poggini, M. Mannini, M. Chiesa, C. Tomasini, F. Pineider, E. Salvadori, S. Carretta, and R. Sessoli, “Direct detection of spin polarization in photoinduced charge transfer through a chiral bridge,” *Chem. Sci.* **13**, 12208–12218 (2022).



- <sup>11</sup>S. Alwan and Y. Dubi, "Spinterface origin for the chirality-induced spin-selectivity effect," *J. Am. Chem. Soc.* **143**, 14235–14241 (2021).
- <sup>12</sup>Y. Dubi, "Spinterface chirality-induced spin selectivity effect in bio-molecules," *Chem. Sci.* **13**, 10878–10883 (2022).
- <sup>13</sup>C. Yang, Y. Li, S. Zhou, Y. Guo, C. Jia, Z. Liu, K. N. Houk, Y. Dubi, and X. Guo, "Real-time monitoring of reaction stereochemistry through single-molecule observations of chirality-induced spin selectivity," *Nat. Chem.* **15**, 972 (2023).
- <sup>14</sup>N. E. Horwitz, B. T. Phelan, J. N. Nelson, M. D. Krzyaniak, and M. R. Wasielewski, "Picosecond control of photogenerated radical pair lifetimes using a stable third radical," *J. Phys. Chem. A* **120**, 2841–2853 (2016).
- <sup>15</sup>N. E. Horwitz, B. T. Phelan, J. N. Nelson, C. M. Mauck, M. D. Krzyaniak, and M. R. Wasielewski, "Spin polarization transfer from a photogenerated radical ion pair to a stable radical controlled by charge recombination," *J. Phys. Chem. A* **121**, 4455–4463 (2017).
- <sup>16</sup>M. T. Colvin, R. Carmieli, T. Miura, S. Richert, D. M. Gardner, A. L. Smeigh, S. M. Dyar, S. M. Conron, M. A. Ratner, and M. R. Wasielewski, "Electron spin polarization transfer from photogenerated spin-correlated radical pairs to a stable radical observer spin," *J. Phys. Chem. A* **117**, 5314–5325 (2013).
- <sup>17</sup>B. K. Rugg, M. D. Krzyaniak, B. T. Phelan, M. A. Ratner, R. M. Young, and M. R. Wasielewski, "Photodrive quantum teleportation of an electron spin state in a covalent donor-acceptor-radical system," *Nat. Chem.* **11**, 981–986 (2019).
- <sup>18</sup>J. N. Nelson, J. Zhang, J. Zhou, B. K. Rugg, M. D. Krzyaniak, and M. R. Wasielewski, "CNOT gate operation on a photogenerated molecular electron spin-qubit pair," *J. Chem. Phys.* **152**, 014503 (2020).
- <sup>19</sup>A. Fernandez, E. Moreno Pineda, C. A. Muryn, S. Sproules, F. Moro, G. A. Timco, E. J. L. McInnes, and R. E. P. Winpenny, "g-engineering in hybrid rotaxanes to create AB and AB<sub>2</sub> electron spin systems: EPR spectroscopic studies of weak interactions between dissimilar electron spin qubits," *Angew. Chem., Int. Ed.* **54**, 10858–10861 (2015).
- <sup>20</sup>J. H. Olshansky, J. Zhang, M. D. Krzyaniak, E. R. Lorenzo, and M. R. Wasielewski, "Selectively addressable photogenerated spin qubit pairs in DNA hairpins," *J. Am. Chem. Soc.* **142**, 3346–3350 (2020).
- <sup>21</sup>B. K. Rugg, K. E. Smyser, B. Fluegel, C. H. Chang, K. J. Thorley, S. Parkin, J. E. Anthony, J. D. Eaves, and J. C. Johnson, "Triplet-pair spin signatures from macroscopically aligned heteroacenes in an oriented single crystal," *Proc. Natl. Acad. Sci. U. S. A.* **119**, e2201879119 (2022).
- <sup>22</sup>C. D. Aiello, J. M. Abendroth, M. Abbas, A. Afanasev, S. Agarwal, A. S. Banerjee, D. N. Beratan, J. N. Belling, B. Berche, A. Botana, J. R. Caram, G. L. Celardo, G. Cuniberti, A. Garcia-Etxarri, A. Dianat, I. Diez-Perez, Y. Guo, R. Gutierrez, C. Herrmann, J. Hihath, S. Kale, P. Kurian, Y.-C. Lai, T. Liu, A. Lopez, E. Medina, V. Mujica, R. Naaman, M. Noormandipour, J. L. Palma, Y. Paltiel, W. Petuskey, J. C. Ribeiro-Silva, J. J. Saenz, E. J. G. Santos, M. Solyanik-Gorgone, V. J. Sorger, D. M. Stemer, J. M. Ugalde, A. Valdes-Curiel, S. Varela, D. H. Waldeck, M. R. Wasielewski, P. S. Weiss, H. Zacharias, and Q. H. Wang, "A chirality-based quantum leap," *ACS Nano* **16**, 4989–5035 (2022).
- <sup>23</sup>R. Haberkorn, "Density matrix description of spin-selective radical pair reactions," *Mol. Phys.* **32**, 1491–1493 (1976).
- <sup>24</sup>J. Fransson, "Chirality-induced spin selectivity: The role of electron correlations," *J. Phys. Chem. Lett.* **10**, 7126–7132 (2019).
- <sup>25</sup>K. Bader, D. Dengler, S. Lenz, B. Endeward, S.-D. Jiang, P. Neugebauer, and J. van Slageren, "Room temperature quantum coherence in a potential molecular qubit," *Nat. Commun.* **5**, 5304 (2014).
- <sup>26</sup>M. Atzori, E. Morra, L. Tesi, A. Albino, M. Chiesa, L. Sorace, and R. Sessoli, "Quantum coherence times enhancement in vanadium(IV)-based potential molecular qubits: The key role of the vanadyl moiety," *J. Am. Chem. Soc.* **138**, 11234–11244 (2016).
- <sup>27</sup>J. M. Zadrozny, J. Niklas, O. G. Poluektov, and D. E. Freedman, "Millisecond coherence time in a tunable molecular electronic spin qubit," *ACS Cent. Sci.* **1**, 488 (2015).
- <sup>28</sup>C.-J. Yu, M. J. Graham, J. M. Zadrozny, J. Niklas, M. D. Krzyaniak, M. R. Wasielewski, O. G. Poluektov, and D. E. Freedman, "Long coherence times in nuclear spin-free vanadyl qubits," *J. Am. Chem. Soc.* **138**, 14678–14685 (2016).
- <sup>29</sup>J. M. Zadrozny and D. E. Freedman, "Qubit control limited by spin-lattice relaxation in a nuclear spin-free iron(III) complex," *Inorg. Chem.* **54**, 12027–12031 (2015).
- <sup>30</sup>M. J. Graham, J. M. Zadrozny, M. Shiddiq, J. S. Anderson, M. S. Fataftah, S. Hill, and D. E. Freedman, "Influence of electronic spin and spin-orbit coupling on decoherence in mononuclear transition metal complexes," *J. Am. Chem. Soc.* **136**, 7623–7626 (2014).
- <sup>31</sup>M. Shiddiq, D. Komijani, Y. Duan, A. Gaita-Ariño, E. Coronado, and S. Hill, "Enhancing coherence in molecular spin qubits via atomic clock transitions," *Nature* **531**, 348–351 (2016).
- <sup>32</sup>J. A. Jones, K. Maeda, and P. J. Hore, "Reaction operators for spin-selective chemical reactions of radical pairs," *Chem. Phys. Lett.* **507**, 269–273 (2011).
- <sup>33</sup>J. A. Jones and P. J. Hore, "Spin-selective reactions of radical pairs act as quantum measurements," *Chem. Phys. Lett.* **488**, 90–93 (2010).
- <sup>34</sup>T. P. Fay, L. P. Lindoy, and D. E. Manolopoulos, "Spin-selective electron transfer reactions of radical pairs: Beyond the Haberkorn master equation," *J. Chem. Phys.* **149**, 064107 (2018).
- <sup>35</sup>Y. E. Kandrashkin and K. M. Salikhov, "Numerical simulation of quantum teleportation across biological membrane in photosynthetic reaction centers," *Appl. Magn. Reson.* **37**, 549–566 (2010).
- <sup>36</sup>S. M. Harvey and M. R. Wasielewski, "Photogenerated spin-correlated radical pairs: From photosynthetic energy transduction to quantum information science," *J. Am. Chem. Soc.* **143**, 15508–15529 (2021).
- <sup>37</sup>H. B. Gray and J. R. Winkler, "Long-range electron transfer," *Proc. Natl. Acad. Sci. U. S. A.* **102**, 3534–3539 (2005).
- <sup>38</sup>A. Chiesa, F. Petiziol, M. Chizzini, P. Santini, and S. Carretta, "Theoretical design of optimal molecular qubits for quantum error correction," *J. Phys. Chem. Lett.* **13**, 6468–6474 (2022).
- <sup>39</sup>A. S. Lukas, P. J. Bushard, and M. R. Wasielewski, "Ultrafast molecular logic gate based on optical switching between two long-lived radical ion pair states," *J. Am. Chem. Soc.* **123**, 2440–2441 (2001).
- <sup>40</sup>A. Farazdel, M. Dupuis, E. Clementi, and A. Aviram, "Electric-field induced intramolecular electron transfer in spiro  $\pi$ -electron systems and their suitability as molecular electronic devices. A theoretical study," *J. Am. Chem. Soc.* **112**, 4206–4214 (1990).
- <sup>41</sup>A. Chatterjee, P. Stevenson, S. De Franceschi, A. Morello, N. P. de Leon, and F. Kuemmeth, "Semiconductor qubits in practice," *Nat. Rev. Phys.* **3**, 157–177 (2021).
- <sup>42</sup>C. Kulkarni, A. K. Mondal, T. K. Das, G. Grinbom, F. Tassinari, M. F. J. Mabeoone, E. W. Meijer, and R. Naaman, "Highly efficient and tunable filtering of electrons' spin by supramolecular chirality of nanofiber-based materials," *Adv. Mater.* **32**, 1904965 (2020).
- <sup>43</sup>H. Lu, J. Wang, C. Xiao, X. Pan, X. Chen, R. Brunecky, J. J. Berry, K. Zhu, M. C. Beard, and Z. V. Vardeny, "Spin-dependent charge transport through 2D chiral hybrid lead-iodide perovskites," *Sci. Adv.* **5**, eaay0571 (2019).
- <sup>44</sup>Y. Lu, Q. Wang, R. He, F. Zhou, X. Yang, D. Wang, H. Cao, W. He, F. Pan, Z. Yang, and C. Song, "Highly efficient spin-filtering transport in chiral hybrid copper halides," *Angew. Chem., Int. Ed.* **60**, 23578–23583 (2021).
- <sup>45</sup>U. Huizi-Rayo, J. Gutierrez, J. M. Seco, V. Mujica, I. Diez-Perez, J. M. Ugalde, A. Tercjak, J. Cepeda, and E. San Sebastian, "An ideal spin filter: Long-range, high-spin selectivity in chiral helicoidal 3-dimensional metal organic frameworks," *Nano Lett.* **20**, 8476–8482 (2020).
- <sup>46</sup>S. L. Bayliss, D. W. Laorenza, P. J. Mintun, B. D. Kovos, D. E. Freedman, and D. D. Awschalom, "Optically addressable molecular spins for quantum information processing," *Science* **370**, 1309–1312 (2020).
- <sup>47</sup>S. L. Bayliss, P. Deb, D. W. Laorenza, M. Onizhuk, G. Galli, D. E. Freedman, and D. D. Awschalom, "Enhancing spin coherence in optically addressable molecular qubits through host-matrix control," *Phys. Rev. X* **12**, 031028 (2022).
- <sup>48</sup>A. Chiesa, S. Roca, S. Chicco, M. C. de Ory, A. Gómez-León, A. Gomez, D. Zueco, F. Luis, and S. Carretta, "Blueprint for a molecular-spin quantum processor," *Phys. Rev. Appl.* **19**, 064060 (2023).